Proceedings World Geothermal Congress 2020+1
Reykjavik, Iceland, April - October 2021

Seismic Velocity Variations Associated with Fluid Injection Stimulation Based on Seismic Ambient Noise Interferometry at Pohang EGS Site, Korea

Lanbo Liu[1], Kwang-Hee Kim[2], and Su Young Kang[2]

[1]Department of Geosciences, University of Connecticut, Storrs, Connecticut, USA

[2]Department of Geological Sciences, Pusan National University, Busan, Korea

Lanbo.Liu@UConn.edu, kwanghee@pusan.ac.kr, sukang@pusan.ac.kr

Keywords: Pohang EGS site, injection stimulation, induced seismicity, ambient noise interferometry, seismic velocity variations

ABSTRACT

The November 15, 2017 M_w5.5 earthquake occurred near the Pohang, EGS site, Korea is the largest known induced/triggered event at an EGS site (Kim et al, 2018). Within 10 km from the Pohang EGS site there is a permanent seismic station (PHA2) operating continuously before this major event. Using the 3-component continuous seismic record from this station we assessed the relative variation of the seismic velocity based on ambient noise interferometry. Auto-correlation functions (ACFs) and single-station, cross-component cross-correlation functions (SCFs) of the 3-component records generate 6 independent time series (EE, NN, ZZ, EN, NZ and ZE) using a 30-sec time window. These interferometric results can be regarded as the pulse-echo situation, i.e., the source and receiver are co-located at this seismic station (e.g., Claerbout, 1968) to ping and receive information from the seismogenic area in the vicinity of the Pohang EGS site. Using the stretching method (e.g., Lobkis and Weaver, 2003; Sens-Schönfelder and Wegler, 2006) we can convert the relative travel time change *dt/t* to the relative velocity change *dv/v*. After an experiment using a testing period in 2015-2016, a period of 326 days (9/11/2016-8/4/2017) continuous records at PHA2 were used to search the relative velocity change *dv/v* and its possible link with changes in pore pressure and/or fault zone property resulted from EGS operation. In this period of time two injection stimulations (G1-1 in Well PX-1, and G2-2 in Well PX-2, see Woo et al, 2019) were conducted at Pohang EGS. The relative velocity *dv/v* displays ~ 0.2% increase for both stimulations. However, it seems an impulse response for G1-1 in PX-1, whose well head is above the seismogenic fault; while a durable, persistent increase for G2-2 in PX-2, whose well head is below the fault. The observed 0.2% velocity change is well above the detection threshold of 0.01%, as calibrated by the velocity response to the tidal strain (Sens-Schönfelder and Eulenfeld, 2019). This work demonstrates that ambient noise observation and interferometry is very sensible to subtle subsurface condition changes. It has the potential to provide a cost-effective means for continuous monitoring EGS operation safety and potential of induced seismicity at EGS sites with well-planned observation array and advanced signal processing schemes in the future.

1. INTRODUCTION

The 2017 M_w 5.5 Pohang earthquake in South Korea is the first reported and largest magnitude induced earthquake in Korea. It occurred near the enhanced geothermal power plant in Pohang on November 15, 2017 (Kim et al., 2018; Lim et al., 2020). The focal depth is estimated to be relatively shallow, at about 4.3 km (KGC, 2019), synthetic aperture radar interferometry (InSAR) constrains the static slip model (Song & Lee, 2019), showing a major slip northeast of the hypocenter.

At the Pohang EGS site, all available lines of evidence including the temporal relationship between seismicity and fluid injection, the spatial relationship between the hypocenters and the EGS site, as well as the lack of seismicity in the area before the EGS drilling and manipulation confirm that the irrupting increase of micro-seismicity was induced and the M_w 5.5 main event was triggered by the EGS operation at the Pohang site (Kim et al., 2018; Grigoli et al., 2018; KGC, 2019). Furthermore, the immediate response of seismicity to fluid injection and the locations of the foreshocks and mainshock at the bottom of the injection well suggest that fluid was injected directly into a fault zone through EGS borehole PX-2. The fault plane inferred from the spatial distribution of hypocenters and focal mechanism solutions strikes NE and dips to the NW, similar to most Quaternary thrust faults in southeastern Korea. Moreover, a magnetotelluric survey at the EGS site also detected a low-resistivity feature that could be the fault zone, striking NE and dipping to the NW, fundamentally in agreement with the fault orientation defined by the distribution of the seismicity. Reverse slip along a subsurface fault is consistent with the current tectonic stress field in the Korean Peninsula.

Lim et al. (2020) showed that the delay between the injection and the Pohang earthquake requires diffusivity estimates within a range of 1-5 × 10^{-4} m^2/s for damaged granodiorite at the focal depth of 4–5 km. Westaway and Burnside (2019) showed that hydrochemical changes occurring while surface water, injected into granite, re-equilibrates chemically with its subsurface environment, can account for time delays for earthquake occurrence of such duration, provided the seismogenic fault was already critically stressed, or very close to the condition for slip. This candidate causal mechanism counters the potential argument that the time delay militates against an anthropogenic cause of the Pohang earthquake and can account for its relatively large magnitude as a consequence of a relatively small-volume injection. The resulting analysis places bounds on combinations of physical and chemical properties of rocks, injected volume, and potential post-injection time delays for significant anthropogenic seismicity during future EGS projects in granite. However, McClure and Horne (2014) made cautions for the complexity of the situation when conduct assessments using fault development at the wellbore to predict induced seismicity hazard. Variations in frictional properties might be unrelated to the degree of fault development.

The aforementioned in-depth analyses and studies from tectonophysics, seismology, hydrogeology, drilling engineering and geochemistry have provided excellent constraints to enable the researchers to understand the seismogenic process that leads to the occurrence of the M_w 5.5 main event. In this paper we look into the seismic wave velocity variations associated with EGS operation at the Pohang EGS site through continuous seismic ambient noise observations.

Numerous studies have demonstrated and approved that the existence of persistent and extensive seismic noise allows us to reconstruct the propagation Green's function by continuously cross- or auto-correlating seismic ambient noise records. With long-term observations, this noise also allows us to monitor the seismic wave velocity changes with time. By measuring the changes in seismic velocity, we can investigate the stress state of the crust at depth and continuously in time, which provides essential constraints on dynamic processes in the crust, such as those attributable to earthquakes (e.g., Rohrbach et al., 2013; Hobiger et al., 2014; Nimiya et al., 2017), volcanoes (e.g., Sens-Schönfelder and Wegler, 2006; Brenguier et al., 2011; De Plaen et al., 2016; De Plaen et al., 2016), and other activities (e.g., Wegler and Sens-Schönfelder, 2007). Nevertheless, there are few reports discuss on monitoring tectonophysics and seismogenic processes by seismic velocity variations using ambient noise data at an EGS site. In this paper we use the continuous seismic ambient noise data at station PHA2 to look into the EGS operation related seismic velocity variations.

In the following sections we first briefly summarize the observation condition at station PHA2. Then we give a quick survey of the method used to extract the relative seismic velocity changes using ambient noise. Next we present the main findings of the velocity change associated with Pohang EGS operation at a couple of injection stimulations. We validate the findings by arguing that the seismic velocity variation even responds to earth tides whose effect is at least one order of magnitude than that of the EGS operation. Finally, we discuss the possible hypothesis of the tectonic and seismogenic cause to the observed velocity variations in the Result Discussion section, and wrap up with restating the major findings and pointing out the potential future study in Conclusion.

2. SEISMIC VELOCITY VARIATIONS FROM AMBIENT NOISE INTERFEROMETRY

At the Pohang EGS site, five hydraulic stimulations were conducted in PX-1 and PX-2 between January 29, 2016 and September 18, 2017, prior to the occurrence of the M_w 5.5 major event on November 15, 2017 (Figure 1A). The first, third, and fifth stimulations were conducted in PX-2 well and the second and fourth in PX-1 well (Figure 1B). Each hydraulic stimulation involved multiple periods of injection, when water is forced into the formation under a wellhead pressure and repeated periods of shut-in or water flowing back to the surface. Available information from drilling and EGS operation indicated out that the injection conditions in the two wells were quite different, requiring a maximum well-head pressure of 24 MPa (a sub-hydrostatic condition) in PX-1 and almost 90 MPa (a sub-lithostatic condition) in PX-2 (KGC 2019). That implies the pore pressure has 4 times difference at the same depth on the opposite sides of the seismogenic fault that accommodates the pending M_w 5.5 event. The Pohang earthquake occurred during shut-in of PX-1 and flow-back of PX-2 after the fifth stimulation. All of these facts imply that the fault at the EGS site is quite impermeable or a fault seal before the major event.

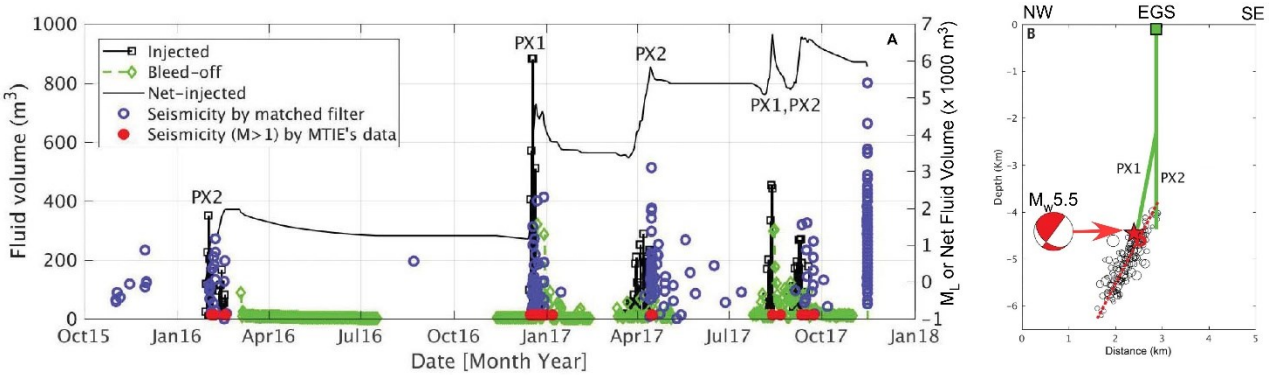

Figure 1: History of fluid injection volume and associated seismicity (A) and relative position of the seismicity, location of the M_w5.5 main shock, and the EGS wells Px-1 and Px-2 (B, based on Kim et al., 2018). Volume of injected and bleed-off fluid (left axis of A) and net fluid volume (right axis of A) as a function of time. Red circles denote times of seismic events from data provided by the MTIE (63 events; magnitude information is only available for M > 1). Dark blue circles denote seismic events determined by matched-filter analysis (148 events). The right axis of A also gives the local magnitude (M_L) of seismic events.

Correlation operation among 3-component continuous seismic records can generate 3 independent auto correlation functions (ACFs for EE, NN, and ZZ) and 3 single-station cross-correlation functions (SCFs, for EN, NZ and ZE). ACFs and SCFs at a single station can be regarded as the situation for equivalent pulse-echo or zero-offset reflection, i.e., the source and receiver are co-located at the same seismic station (e.g., Claerbout, 1968; Hobiger, et al., 2014). Using data from a single station is unable to derive the absolute velocity change. Nevertheless, it is able to assess the relative changes in seismic velocity. In this study, we used the continuous ambient noise data from the permanent seismic station PHA2 to extract the relative variation in seismic velocity.

2.1 The PHA2 Station

Station PHA2 (Figure 2) is located at 36º11'59", 129º22'11" (36.1997º, 129.3697º) with an elevation of 12 m. it is about 10 km due north of the Pohang EGS site, on the coastal shore line of East Sea (Sea of Japan). The sampling rate of the continuous seismic record at PHA2 is 100 Hz. Continuous data are available as early as 2014. Unfortunately, there are a number of data gaps that interrupted the data continuity, which prevents for computing relative velocity variations in a longer period of time. Therefore, we have to use some segments that cover the EGS injection episodes under investigation as long as possible, especially prior to the stimulation injection. A segment of the original 3-component ambient noise data is shown as the inset in Figure 2.

2.2 Computation of the Relative velocity change dv/v from Single Station Ambient Noise Record

We are interested in estimating the relative changes in seismic velocity of the medium (dv/v) using cross-correlations (CC) of noisy recordings. We first construct two CC functions: the reference CC, i.e., CC_{ref}, which is computed using all the available data; and the

current CC, i.e., CC_{cur}, which is computed by averaging the hourly CC function over a few hours around the current hour we want to conduct the measurement on. The two CC functions are used in Stretching Method (Lobkis and Weaver, 2003; Sens-Schönfelder and Wegler, 2006) to estimate the relative velocity changes *dv/v*. SM searches the coefficient ε that maximizes C(ε) defined as:

$$C(\varepsilon) = \frac{\int CC_{cur}(t(1+\varepsilon))CC_{cur}(t)dt}{\sqrt{(\int CC_{cur}(t(1+\varepsilon))^2 dt)(\int CC_{ref}(t)^2 dt)}} \quad (2)$$

Essentially, the stretching method works by optimizing the correlation coefficient between any two comparable correlation functions after deforming one of them with a stretching coefficient. The changes in seismic velocity are equal to the stretching coefficient producing the maximum cross-correlation coefficient. Using the stretching method we can convert the relative travel time change *dt/t* to relative velocity change *dv/v*., i.e.:

$$\varepsilon = \frac{dt}{t} = -\frac{dv}{v} \quad (3)$$

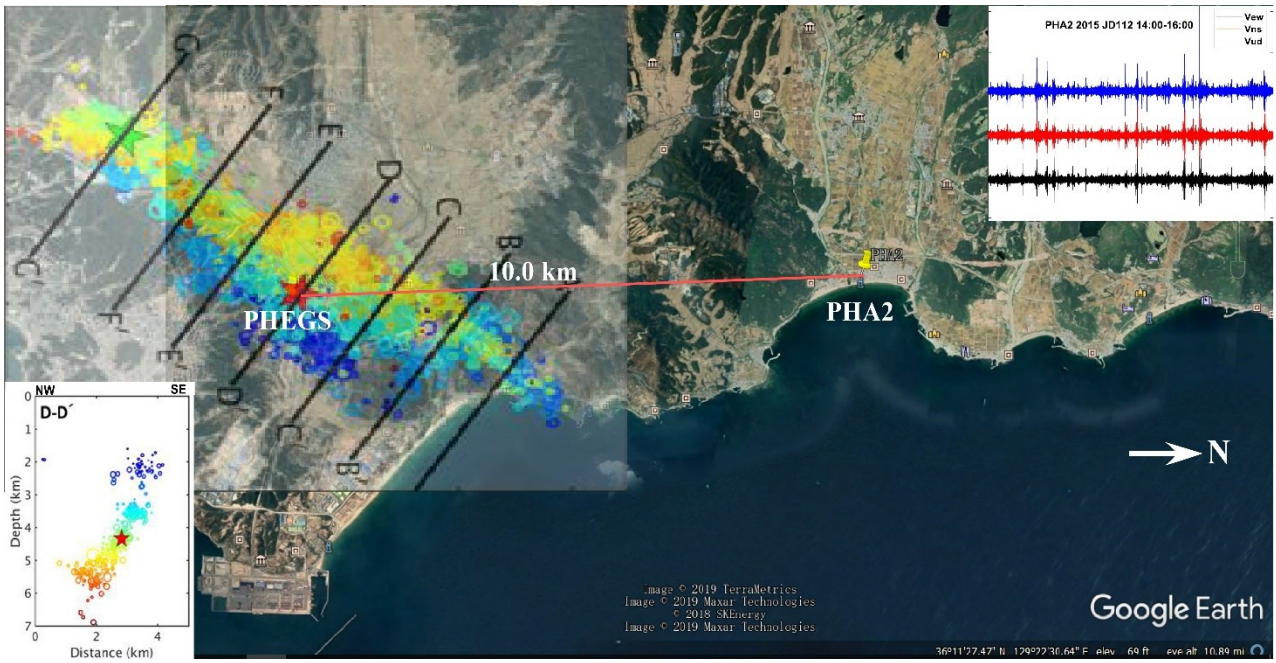

Figure 2: The relative position of the station PHA2 and the Pohang EGS site (PHEGS, the red star). The direct distance between PHA2 and PHEGS is about 10 km. The distribution of the seismicity (Kim, et al., 2020) is superimposed on the Google Earth image. The lower left inset of the figure gives the vertical distribution and the location of the main shock on cross-section DD' (Kim, et al., 2020). The upper right inset shows a period of 2 hours 3-component ambient noise data recorded in Julian day 112 (April 22) of 2015 at PHA2.

Sens-Schönfelder and Eulenfeld (2019) have found that the filtered correlation functions for the range of 3-7 Hz generated the highest signal to noise ratio velocity variation; we thus follow their approach to using the filtered CC in the same frequency range to seek the relative variation in seismic velocity. We use one whole hour of continuous seismic records at PHA2, then carry out the correlations with an elapse window of 30 seconds; that implies an amount of 120 independent superposition stacks can be used to improve the signal to noise ratio. We think a window of 30 seconds in long enough as the two-way travel time for the slowest possible seismic wave to virtually propagates from the station PHA2 to the seismogenic zone beneath Pohang EGS and reflected back to PHA2. A set of the typical ACFs for EE, NN, and ZZ and SCFs, for EN, NZ and ZE is shown in Figure 3. We used the coda portion of 10-30 sec of the ACFs to examine the possible velocity variations, for its assurance to reach to 10 km even by the slowest possible seismic waves.

For the data processing we first eliminate the DC constituent of the ambient noise data by subtracting the mean of the records in the 3 components. Then we setup a threshold limit to exclude the spiking outliers. Next, we use the one-bit correlation to carry out the main data processing to generate the correlation functions using one hour ambient noise data, with a correlation window of 30 seconds and a sliding interval of 15 seconds so that most of the data points in one hour have been used twice to generate ACFs and SCFs. The ACFs and SCFs are then band-pass filtered to 3-7 Hz using a 4^{th}-order Butterworth filter, then carry out the relative velocity analysis using the stretching method (Lobkis and Weaver, 2003; Sens-Schönfelder and Wegler, 2006).

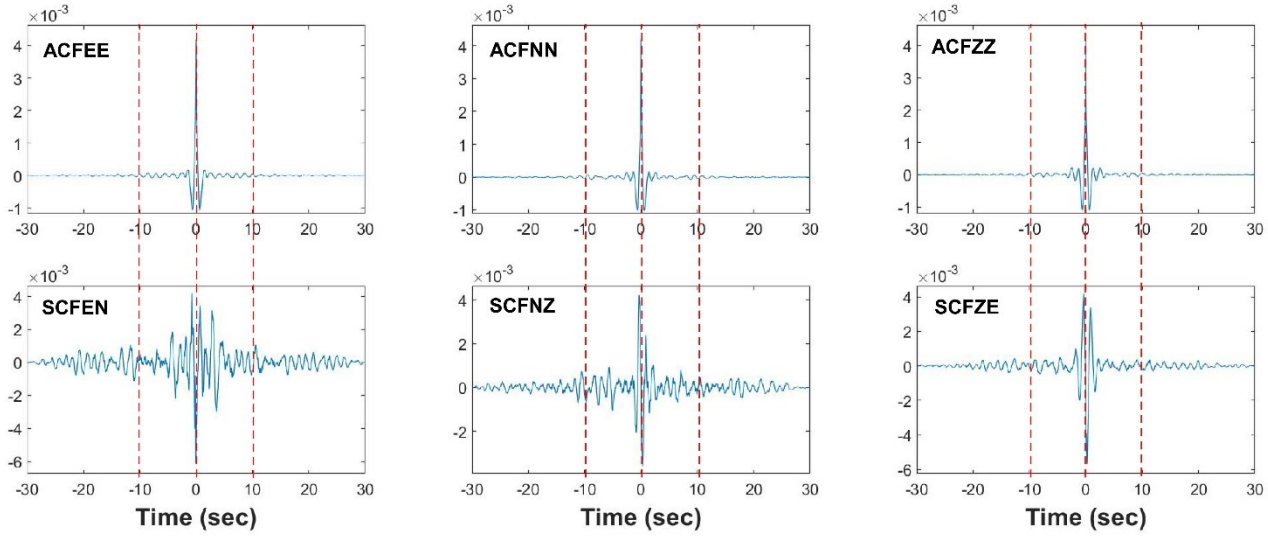

Figure 3: Typical ACFs and SCFs with a window length of 30 seconds using one hour 3-component ambient noise data from the seismic record at PHA2. The coda in 10-30 sec of the ACFs are used to examine the possible velocity variations.

2.3 Calibration with Earth Tides

The confidence level of the relative velocity variations associated with potential seismogenic process in the vicinity of a pending earthquake focal region or any regions experiencing pore pressure and stress state perturbation from EGS operation may be examined by its response to some subtler stimulations. If the velocity change can be responding to the subtler stimulation source, it can be reasonably assume that it should respond to the stimulation as a higher level. Tidal deformation can be such an ideal candidate to provide such a subtle, definitive stimulation (Liu, 1984) to be used to scrutinize the response of the seismic velocity variations. Tidal strain can reach the magnitude of several tens of Nano-strain (~10s x 10^{-9}). The sensitivity of the relative velocity change to tidal strain is about 10^4 (Sens-Schönfelder and Eulenfeld, 2019), i.e., ten nano-strain (10^{-8}) can generate 0.01% (10^{-4}) relative change in seismic velocity. This order of magnitude of seismic velocity response to tidal strain is also confirmed and validated by field experiments using seismic network pinged by a continuous active source (Wang et al, 2020) and ambient noise observations (Sens-Schönfelder and Eulenfeld, 2019). Using tides as a calibration, Deplaen et al. (2019) found +/-0.3% variation in *dv/v* associated with volcano eruption at Mt. Etna. Thus, the level of the observed *dv/v* variations at the order of a few times 10^{-3} (about 10 time of the detection threshold demonstrated by the response to tidal strain) associated with seismogenic, volcanic, and EGS operation is plausibly trustable with a significant level of signal to noise ratio.

The comparison of the relative velocity variations and the tidal dilation, along with the spectrum of the velocity changes are presented for the period of September 1, 2015 to February 15, 2016 in Figure 4, and the for the period of September 11, 2016 to August 4, 2017 in Figure 5. From the spectrum we can clearly see that the diurnal solar tide constituent (S_1) is the most pronounced frequency component for both segments. We can also marginally see the energy at the semi-diurnal frequency at 0.08/h (equivalent to the period of 12^h25^m) which should be the M_2 tide in the velocity variation spectrum for the second observation segment for 2016-2017 (Figure 5). The reason for a much stronger diurnal effect is possibly due to the daily variation in temperature at station PHA2.

3. RESULT DISCUSSIONS

The tidal dilatation values shown in the top panel of Figures 4 and 5 are calculated using standard approach with the Longman formula (Liu, 1984). The variations of the relative variation in seismic velocity extracted by the stretching method (Lobkis and Weaver, 2003; Sens-Schönfelder and Wegler, 2006) are on the order of 0.1%, with the maxima of around +/- 0.2%. The *dv/v* variations are extracted from the later time (10-30 seconds) of the coda of the ACFs. To match with the tidal dilatation that might be straightforwardly associated with pore pressure, the three ACFs are combined into one that is proportional to dilatation or mean stress, which is formed the middle panel of Figures 4 and 5. Using spectrum analysis via fast Fourier transform (FFT) we can clearly see the dominating diurnal component in the relative velocity changes.

3.1 The segment of September 1, 2015 to February 15, 2016

For this period of time, we cannot reasonably argue any significant response in relative velocity changes to the first mud loss and the first injection stimulation in PX-2. We suspect that the stress level is still quite distant to failure point. The quality of the seismic velocity variation should be at least or even better than the second segment being discussed in the next sub-section, by the evidence of the significant response to the diurnal tides (S1), as shown in the bottom panel of Figure 4.

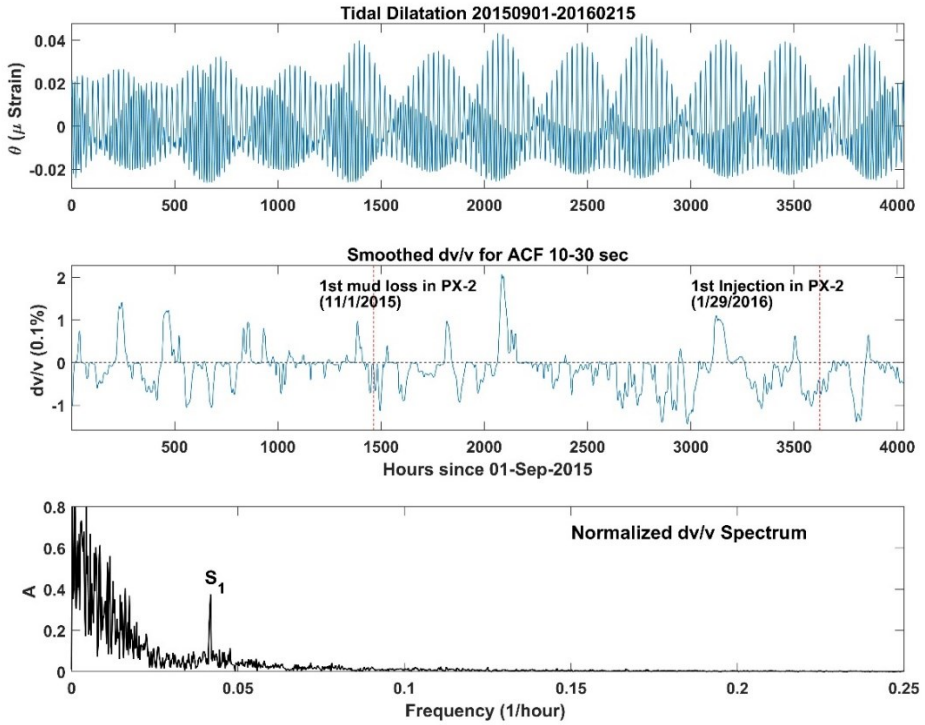

Figure 4: Theoretical tidal dilatation (top panel) at station PHA2, the relative velocity changes computed based on the coda part of 10-30 seconds of the 3-component ACFs at Station PHA2 from the period of September 1, 2015 to February 15, 2016 (middle panel), and the corresponding spectrum of the velocity variation (bottom panel). The occurrence times of the first mud loss in PX-1 and the first injection stimulation in PX-2 are marked as the red broken line.

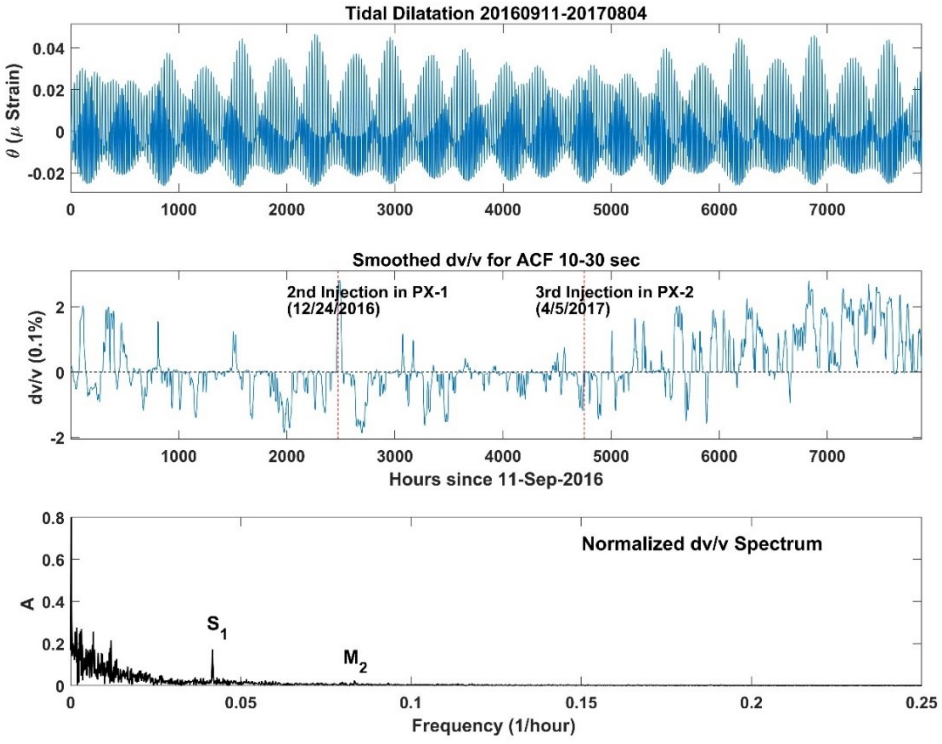

Figure 5: Theoretical tidal dilatation (top panel) at station PHA2, the relative velocity changes computed based on the coda part of 10-30 seconds of the 3-component ACFs at Station PHA2 from the period of September 11, 2016 to August 4, 2017 (middle panel), and the corresponding spectrum of the velocity variation (bottom panel). The occurrence times of the second injection stimulation in PX-1 and the third injection stimulation in PX-2 are marked as the red broken line.

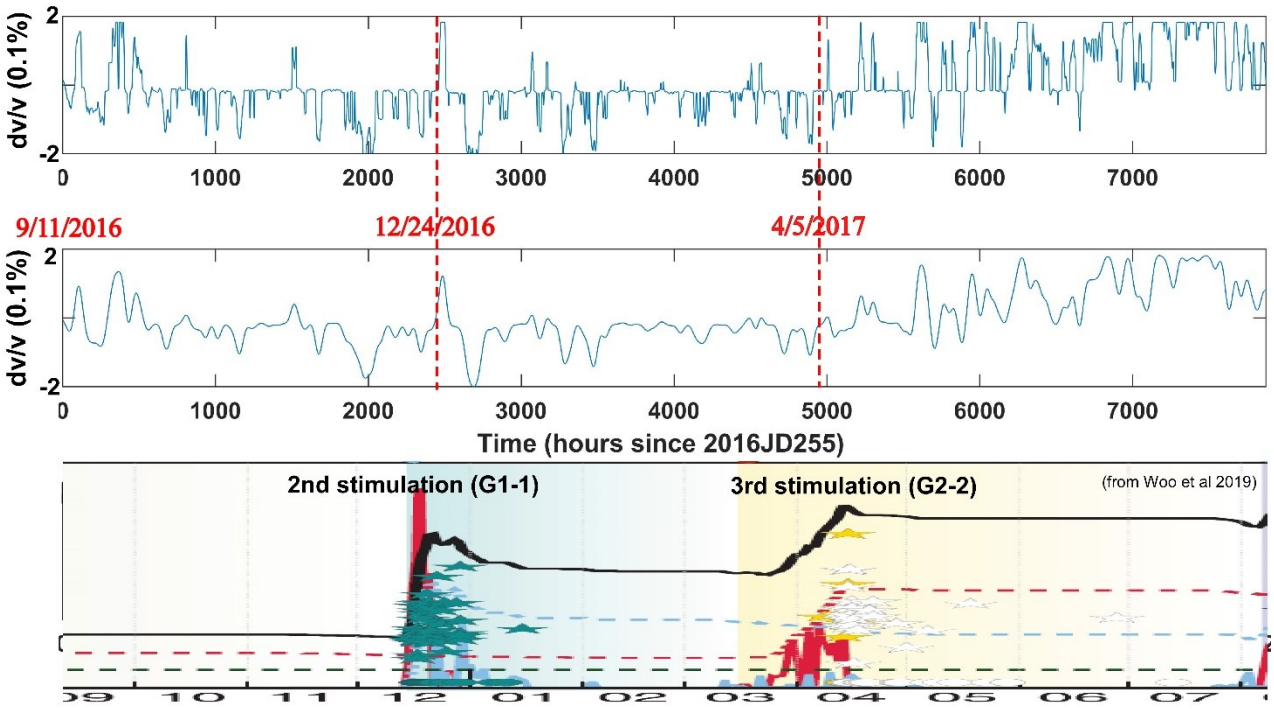

Figure 6: Relative changes in seismic velocity obtained by applying the stretching method using 3-component records at Station PHA2 around the second and third injection simulation in the Pohang EGS Wells for the period of 9/11/2016 to 8/4/2017 during which the second stimulation (G1-1) injected in well PX-1 on 12/24/2016, and the third stimulation (G2-2) injected in Well PX-2 on April 5, 2017. The bottom panel of the injection history is from Woo et al. (2019).

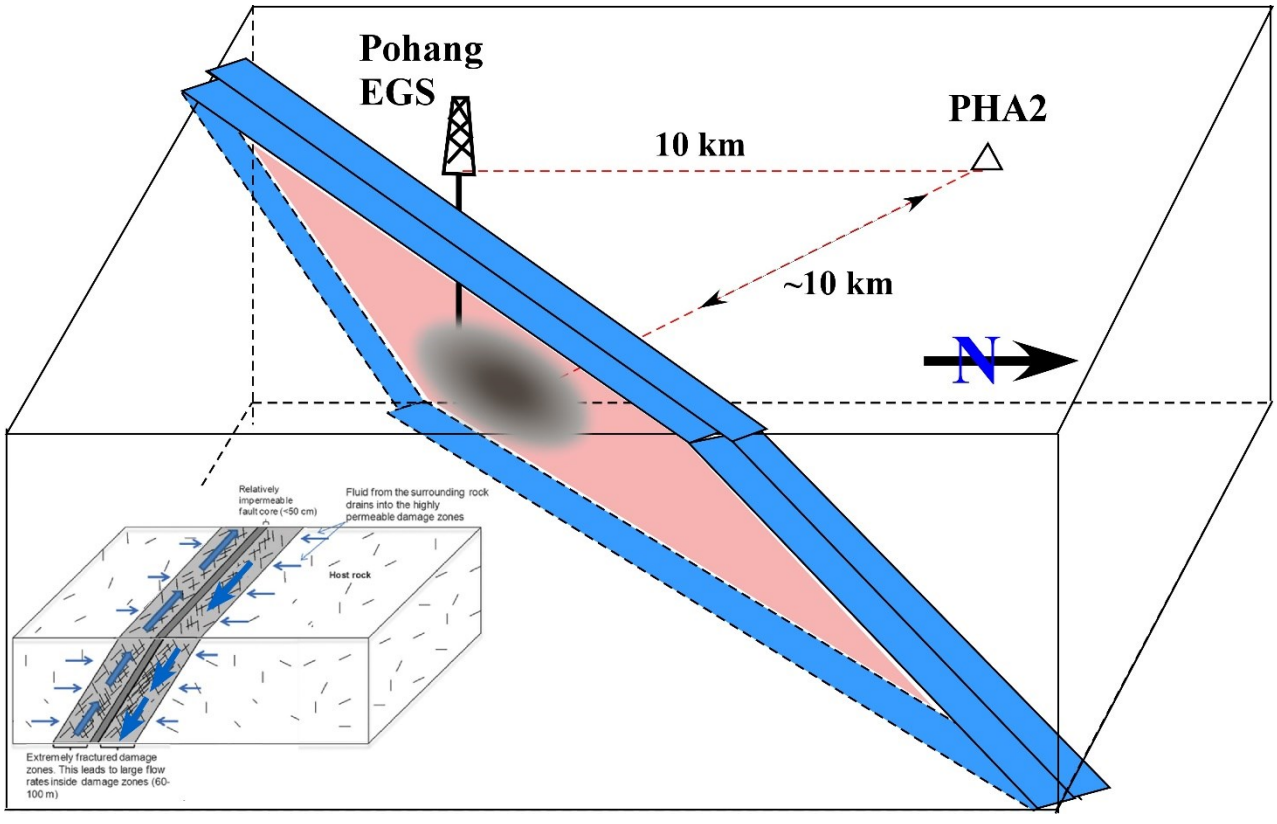

Figure 7: A cartoon to illustrate the station PHA2, the Pohang EGS and the fault containing a region with pore pressure changes. The inset of the fault model is modified from Johri et al. (2014).

3.2 The segment of September 11, 2016 to August 4, 2017

For this second segment of the relative velocity calculation, the velocity response to the second injection stimulation in PX-1 (above the fault) looks like very instantaneous, expressed as a sudden impulse of velocity increase at a magnitude of 0.2%. In contrast, the *dv/v* response to the third injection stimulation in PX-2 (below the fault) displayed a delayed and persistent increase, the magnitude is also can reach 0.2%.

Clearly, compare to the segment of 2015-2016 (Figure 4), the velocity variation in this 2016-2017 segment looks more responsive to the ambient condition (Figures 5 and 6). Interestingly enough, the behavior of the responses to injection stimulation in PX-1 and PX-2 is quite different. For the response in PX-1, it may look more like an elastic/brittle one, while in PX-2, it may look like more varying, with interactions in a more cracked/fractured under more permeable condition and higher stress level after the occurrence of the Mw 3.2 event, the second highest magnitude event beside the Mw 5.5 main shock that associated with the third injection (Figure 6). In fact, EGS operation with well-head pressure as the index, it showed that the injection conditions in the two wells were different, requiring a maximum well-head pressure of 24 MPa in PX-1, and a much higher 90 MPa in PX-2 (KGC, 2019). These physical property changes are most likely related to micro-crack opening, closing, reorienting, and fluids flow in/out of the cracks, as well as the heat/temperature variation influences. Certainly, more specific delineation of the subsurface condition a devolution still need more observation constraints.

Our hypothetic understanding of the situation of the seismic velocity response to the pore pressure and stress state variations associate with EGS operation is illustrated in the cartoon of Figure 7.

Lim et al. (2020) argued that fluid injections at Pohang EGS site can result in a change of the Coulomb stress of up to 0.04–0.11 MPa. In comparison, the maximum magnitude of tidal stress can be safely estimated on the order of 0.002-0.005 MPa. If the relative velocity change in seismic velocity can be affected by tidal strain at this stress level, the ability to sense the stress changes caused by fluid injection at one order of magnitude higher is definitely a reasonable hypothesis.

4. CONCLUSION

With the relative velocity change in the first segment of 2015-2016 as the reference, velocity changes in the period of 2016-2017 can be examined against two injection stimulations (G1-1 in Well PX-1, and G2-2 in Well PX-2, see Woo et al, 2019) conducted at the Pohang EGS site. The relative velocity *dv/v* displays ~ 0.2% increase for both stimulations. However, it seems an impulse response for G1-1 in PX-1, whose well head is above the seismogenic fault; while a durable, persistent increase for G2-2 in PX-2, whose well head is below the fault. The observed 0.2% velocity change is well above the detection threshold of 0.01%, as calibrated by the velocity response to the tidal strain (Sens-Schönfelder and Eulenfeld, 2019). This work demonstrates that ambient noise observations and interferometry are very sensible to subtle subsurface condition changes. It has the potential to provide a cost-effective means for continuous monitoring EGS operation safety and potential of induced seismicity at EGS sites with well-planned observation array and advanced signal processing schemes in the future.

It is reasonable to speculate that rich information exist in the continuous records of a seismic network that can be linked to EGS operations that generate perturbations in pore pressure and tress state variation in the seismogenic depth, especially in the cases that the EGS drilling site is close to a potential blind active fault. The information of velocity change provided by the ambient noise will be especially critical if there is lack of active microseismicities in the vicinity of an EGS site.

REFERENCES

Brenguier, F., Clarke, D., Aoki, Y., Shapiro, N.M., Campillo, M., and Ferrazzini, V.: Monitoring volcanoes using seismic noise correlations, *Comptes Rendus Geosci.,* **343(8-9),** (2011), 633–638.

Claerbout, J.F.: Synthesis of a layered medium from its acoustic transmission response, *Geophysics,* **33,** (1968), 264-269.

De Plaen, R.S.M., Lecocq, T., Caudron, C., Ferrazzini, V., and Francis, O.: Single-station monitoring of volcanoes using seismic ambient noise, *Geophys. Res. Lett.,* **43,** (2016), 8511–8518.

De Plaen, R.S.M., Cannata, A., Cannavo, F., Caudron, C., Lecocq, T., and Francis, O.: Temporal changes of seismic velocity caused by volcanic activity at Mt. Etna revealed by the autocorrelation of ambient seismic noise, *Frontiers in Geoscience*, **6,** (2019), Article 251.

Grigoli, F., Cesca, S., Rinaldi, A., Manconi, A., Lopez-Comino, J., Clinton, J., Westaway, R., Cauzzi, C., Dahm, T., and Wiemer, S.: The November 2017 Mw 5.5 Pohang earthquake: a possible case of induced seismicity in South Korea. *Science,* **360,** (2018), 1003–1006.

Hobiger, M., Wegler, U., Shiomi, K., and Nakahara, H.: Single-station cross-correlation analysis of ambient seismic noise: Application to stations in the surroundings of the 2008 Iwate-Miyagi Nairiku earthquake, *Geophys. J. Int.,* **198,** (2014), 90–109.

Johri, M., Zoback M.D., and Hennings, P.: A scaling law to characterize fault-damage zones at reservoir depths, *AAPG Bulletin,* **98(10),** (2014) 2057–2079.

Kim, K.-H., Ree, J.-H., Kim, Y., Sungshil Kim, S., Kang, S.Y., Seo, W.: Assessing whether the 2017 Mw 5.4 Pohang earthquake in South Korea was an induced event, *Science,* **360**, (2018), 1007–1009.

Kim, K.-H., Seo, W., Han, J., Kwon, J., Kang, S.Y., Ree, J.-H., Kim, S., and Liu, K.: The 2017 M_L5.4 Pohang earthquake sequence, Korea, recorded by a dense seismic network, *Tectonophysics,* **774,** (2020), 228306.

Korean Government Commission on the Cause of the Pohang Earthquake: Summary Report of the Korean Government Commission on Relations between the 2017 Pohang Earthquake and EGS Project, (2019), 205 pp.

Lim, H., Deng, K., Kim, Y.H., Ree, J.-H., Song, T.-R. A., and Kim, K.-H.: The 2017 Mw 5.5 Pohang earthquake, South Korea, and poroelastic stress changes associated with fluid injection. *Journal of Geophysical Research: Solid Earth,* **124,** (2020), e2019JB019134.

Liu, L.: Calculation of theoretical values of the volumetric tidal strain, *Journal of Seismological Research,* **7(6),** (1984), 681-687.

Lobkis, O. I., and Weaver, R. L.: Coda-wave interferometry in finite solids: Recovery of P- to S conversion rates in an elastodynamic billiard, *Physical Review Letters,* **90(25(Pt 1)),** (2003), 254302.

McClure, M.W., and Horne R.N.: Correlations between formation properties and induced seismicity during high pressure injection into granitic rock, *Engineering Geology,* **175,** (2014), 74–80.

Nimiya, H., Ikeda, T., and Tsuji, T.: Spatial and temporal seismic velocity changes on Kyushu Island during the 2016 Kumamoto earthquake, *Sci. Adv.,* **3,** (2017), e1700813.

Rohrbach, E., Liu, L., and Wang, L.: Variations in seismic velocity and attenuation associated with seismogenesis: A numerical verification using ambient noise, *Tectonophysics*, **584**, (2013), 53-63.

Sens-Schönfelder, C., and Wegler, U.: Passive image interferometry and seasonal variations of seismic velocities at Merapi Volcano, Indonesia, *Geophys. Res. Lett.,* **33(21),** (2006), L21302.

Sens-Schönfelder, C., and Eulenfeld, T.: Probing the in situ Elastic Nonlinearity of Rocks with Earth Tides and Seismic Noise, *Physical Review Letters,* **122,** (2019), Article 138501 1-6.

Song, S. G., & Lee, H.: Static slip model of the 2017 Mw 5.4 Pohang, South Korea, earthquake constrained by the InSAR data, *Seismological Research Letters,* **90,** (2019), 140–148.

Wang, B., Yang, W., Wang, W., Yang, J., Li, X., and Ye, B.: Diurnal and semidiurnal P- and S-wave velocity changes measured using an airgun source. *Journal of Geophysical Research: Solid Earth,* **125,** (2020), e2019JB018218.

Wegler, U., and Sens-Schönfelder, C.: Fault zone monitoring with passive image interferometry, *Geophys. J. Int.,* **168,** (2007), 1029–1033.

Westaway, R., and Burnside, N.M.: Fault "Corrosion" by Fluid Injection: A Potential Cause of the November 2017 Mw 5.5 Korean Earthquake, *Geofluids,* (2019), 1280721.

Woo, J.-U., Kim, M., Sheen, D.-H., Kang, T.-S., Rhie, J., Grigoli, F., Ellsworth, W.L., and Giardini, D.: An in-depth seismological analysis revealing a causal link between the 2017 MW 5.5 Pohang earthquake and EGS project, *Journal of Geophysical Research: Solid Earth,* **124,** (2019), 2019JB018368